Received: 13 June 2020 | Revised: 8 December 2020 | Accepted: 10 December 2020

DOI: 10.1111/ejn.15092

RESEARCH REPORT

EJN European Journal of Neuroscience FENS WILEY

# An ultrastructural connectomic analysis of a higher-order thalamocortical circuit in the mouse

**Vandana Sampathkumar** | **Andrew Miller-Hansen** | **S. Murray Sherman** | **Narayanan Kasthuri**

Department of Neurobiology, University of Chicago, Chicago, IL, USA

**Correspondence**
S. Murray Sherman and Narayanan Kasthuri, Department of Neurobiology, University of Chicago, Chicago, IL 60637, USA.
Email: msherman@bsd.uchicago.edu; bobbykasthuri@uchicago.edu

**Funding information**
National Institutes of Health, Grant/Award Number: EY022388, NS094184 and NS113922; National Institute of Mental Health, Grant/Award Number: MH109100; National Eye Institute, Grant/Award Number: EY028812

## Abstract

Many studies exist of thalamocortical synapses in primary sensory cortex, but much less in known about higher-order thalamocortical projections to higher-order cortical areas. We begin to address this gap using genetic labeling combined with large volume serial electron microscopy (i.e., "connectomics") to study the projection from the thalamic posterior medial nucleus to the secondary somatosensory cortex in a mouse. We injected into this thalamic nucleus a cocktail combining a *cre*-expressing virus and one expressing *cre*-dependent ascorbate peroxidase that provides an electron dense cytoplasmic label. This "intersectional" viral approach specifically labeled thalamocortical axons and synapses, free of retrograde labeling, in all layers of cortex. Labeled thalamocortical synapses represented 14% of all synapses in the cortical volume, consistent with previous estimates of first-order thalamocortical inputs. We found that labeled thalamocortical terminals, relative to unlabeled ones: were larger, were more likely to contain a mitochondrion, more frequently targeted spiny dendrites and avoided aspiny dendrites, and often innervated larger spines with spine apparatuses, among other differences. Furthermore, labeled terminals were more prevalent in layers 2/3 and synaptic differences between labeled and unlabeled terminals were greatest in layers 2/3. The laminar differences reported here contrast with reports of first-order thalamocortical connections in primary sensory cortices where, for example, labeled terminals were larger in layer 4 than layers 2/3 (Viaene et al., 2011a). These data offer the first glimpse of higher-order thalamocortical synaptic ultrastructure and point to the need for more analyses, as such connectivity likely represents a majority of thalamocortical circuitry.

**Abbreviations:** AAV, Adeno-associated virus; DV, Dorso-Ventral; ML, Medio-Lateral; AP, Antero-Posterior; APX-C, Cytoplasmic Targeted Ascorbate peroxidase; APEX2, Engineered Ascorbate peroxidase; ATUM, Automatic Tape-collecting Ultramicrotome; DAB, Di-Amino-Benzidine; FOV, Field of View; $H_2O_2$, Hydrogen Peroxide; L1, Layer 1; L2/3, Layer 2/3; L4, Layer 4; L5, Layer 5; L6, Layer 6; POm, Posterior medial nucleus of the thalamus; PSD, Postsynaptic density; S2, Second somatosensory cortical area; M1, Primary motor cortical area; VPm, Ventral Posteromedial nucleus of thalamus; S1, Primary somatosensory cortical area; SEM, Scanning Electron Microscope.

Edited by: Dr. László Acsády

## 1 | INTRODUCTION

Classification of thalamic nuclei into first- and higher-order relays was an important step in understanding principles of thalamocortical interactions (Sherman, 2016; Sherman & Guillery, 2013)). In this scheme, first-order thalamic nuclei transmit information from a subcortical source to primary cortical areas (e.g., retinal input to lateral geniculate nucleus to primary visual cortex), and higher-order nuclei transmit information from layer 5 neurons of one cortical area to another (e.g., as is the case for much of pulvinar and corticocortical communication between primary visual cortex and secondary visual areas). Because all cortical areas receive an input from thalamus and because higher-order thalamic nuclei underlie much of this trans-thalamic corticocortical processing (Sherman, 2016; Sherman & Guillery, 2013), it is of obvious importance to better understand the functional organization of higher-order thalamocortical circuitry. Such an understanding inevitably relies heavily on morphological analysis, and the "gold standard" for morphologically identifying neuronal connections remains electron microscopy. However, to date all or nearly all such studies have focused on first-order thalamocortical pathways, primarily from the lateral geniculate nucleus to primary visual cortex (Ahmed et al., 1994; Anderson et al., 2009; Hornung & Garey, 1981; Peters & Feldman, 1977; Peters et al., 1976) and the ventral posterior nucleus to primary somatosensory cortex (White & Rock, 1979; Hersch & White, 1981; White et al., 2004; Rah et al., 2013; Bopp et al., 2017; Rodriguez-Moreno et al., 2018; Motta et al., 2019; but see Zhou et al., 2018; Chomsung et al., 2010). What is sorely needed are ultrastructural data from further examples of higher-order thalamocortical circuitry.

To begin to address this, we have undertaken an ultrastructural analysis of the higher-order thalamocortical pathway from the posterior medial nucleus to the second somatosensory area in a mouse. To do so, we paired recent advances in engineering proteins for electron-dense genetic labeling with automated large volume serial electron microscopy (Kasthuri et al., 2015; Lam et al., 2015; Martell et al., 2017) to clearly identify the terminals and synapses of these higher-order thalamocortical neurons in all layers of secondary somatosensory cortex.

Our findings include evidence for significant differences between labeled thalamocortical terminals and synapses and unlabeled examples, evidence for laminar variation in the density and synaptic organization of thalamocortical connections, and evidence for differences in some parameters between our analysis of the higher-order relay and prior published data of the first-order relay from the ventral posterior nucleus to the primary somatosensory cortex.

**Significance**

Most thalamocortical projections are from higher-order thalamic nuclei to higher-order cortical areas, yet detailed ultrastructural studies have been mostly limited to first-order projections. To begin to bridge this gap, we used virally mediated labeling and serial electron microscopy to detail a higher-order thalamocortical projection from the posterior medial nucleus to the secondary somatosensory cortical area in the mouse. We document how labeled thalamocortical synapses differ from unlabeled ones, how these vary across cortical layers, and how this pathway differs from first-order projections. This extends our understanding of thalamocortical organization while piloting a useful approach for ultrastructural study of long-range projections. Further, such studies are needed to gain insights into this circuitry, which is so important to cognitive functioning.

Clearly, a better understanding of thalamocortical functioning requires additional characterization of these pathways, and we regard our effort as an early attempt at this effort.

## 2 | Methods

All procedures were performed in accordance with the University of Chicago Institutional Animal Use and Care Committee. Data were obtained from one male wild-type C57/bl6 mouse (JAX).

### 2.1 | Viral injections

We injected a cocktail (1:1 ratio, 60 nL total volume) of two types of AAV using stereotactic coordinates to target the posterior medial nucleus of the thalamus (from bregma in mm: DV, -3.3; ML, +1.3; AP, -1.3; Mo & Sherman, 2019). One virus expressed Cre in local neurons (pENN.AAV1.hSyn.Cre.WPRE.hGH Addgene viral prep # 105553-AAV1) and the second expressed APX-C in a cre-dependent fashion (rAAV9/AAV-CAG-DIO-APEX2NES made at the Gene therapy center vector core at UNC at Chapel Hill). AAV-CAG-DIO-APEX2NES was a gift from Joshua Sanes (Addgene plasmid # 79907; http://n2t.net/addgene:79907; RRID:Addgene_79907).

The mouse was injected with this cocktail at 10 weeks of age, returned to its cage for 4 weeks to allow for transgene expression and transport of the label, and then processed for

peroxidase staining and large volume electron microscopy as described below.

## 2.2 | Electron microscopy

The mouse was heavily anesthetized with pentobarbital (60 mg/kg intraperitoneal) to be non-responsive to toe pinch and transcardially perfused with 50 ml of 0.1M cacodylate buffer followed by 20 ml of buffered 2% paraformaldehyde and 2.5% glutaraldehyde at the rate of 3ml/min. The brain was removed, and vibratome sections (350 μm thick) were cut containing the cortical and thalamic regions of interest using the angle for cutting that maximizes connectivity in somatosensory thalamocortical connections (Agmon & Connors, 1991). The sections were then stained with Di-Amino-Benzidine (DAB) and $H_2O_2$ to visualize APX-C labeling (Joesch et al., 2016). The samples were evaluated at the macro scale for the intensity of the DAB reaction and its localization to the appropriate brain regions, namely, the posterior medial nucleus and second somatosensory cortical area. The posterior medial nucleus was distinguishable by eye, and the second somatosensory cortical area was localized based on its distinctive pattern of labeling via the observed projection from the posterior medial nucleus and its clear border with the primary somatosensory, or barrel cortex. Samples with appropriate staining were subsequently stained with multiple rounds of osmium and reduced osmium, *en bloc* uranium and lead, dehydrated, and then plastic embedded (Hua et al., 2015). Approximately three-thousand 50-nm-thick ultra-thin serial sections were cut with a cross-section of 1.7x1.1 mm, collected on Kapton tape, attached to wafers, and carbon coated (Kasthuri, 2015; Morgan et al., 2016). We subsampled this volume for higher-resolution tracing for each layer: about 200 sections for layers 1, 4, 5, and 6 and 100 sections for layers 2/3. Cortical layers were identified using cytological features like cell size and density and distance from pia and white matter tracts along with reference to the Allen Mouse Brain Atlas (© 2004 Allen Institute for Brain Science. Allen Mouse Brain Atlas, https://mouse.brain-map.org/static/atlas). Briefly, layer 1 was identified by the sparse population of cell bodies, in contrast with layer 2. Layers 2/3 were distinguished by cytoarchitecture and by being sufficiently distant from layers 1 and 4 using distance from pia and the Allen Institute Mouse Atlas. The border between layers 4 and 5 was seen due to a higher cell density in layer 4, and layer 5 can be identified by the presence of large pyramidal cells, in contrast with layers 4 and 6

Ultra-thin sections were then imaged with a backscatter detector on a Zeiss Gemini SEM 300 and ATLAS software. Low-resolution data were imaged at 40 nm x, y pixel resolution and large fields of view were collected by montaging individual tiles (three tiles each of 16k x12k pixels stitched together with 10% overlap to produce a 44.7k x 12k pixel image; because of the 10% overlap; the result is 44.7k x 12k pixels rather than 48k x 12k). Fine-resolution electron microscopic imaging was done at 6 nm resolution and was a single-tile FOV (12k x 12k pixels). Imaging rates were 0.8 μs per pixel for low-resolution images and 1.6 μs /pixel for fine-resolution images. Individual tiles for lower-resolution datasets were stitched in 2D and linearly aligned in 3D using a plugin, TrakEM2 (Cardona et al., 2012), in the open source image processing program *ImageJ*. Fine-resolution image stacks often required further alignment using non-linear deformations of the image, which was performed using the program *aligntk* (https://mmbios.pitt.edu/about-us/acknowledgements) on local desktops.

## 2.3 | Tracing neurons and their connections

For tracing APX-C labeled axons, classifying their postsynaptic targets morphologically, and identifying and characterizing their synaptic features (e.g., measuring spine, terminal, and glia diameters), we used Knossos annotation software (Boergens et al., 2017). For determining density of APX-C labeled terminals and synapses across all layers, we chose three subvolumes of cubes 5 μm on a side in each cortical layer, targeting a vertical zone of the highest APX-C labeling density as identified from the lower-resolution datasets. In these subvolumes, we annotated all unlabeled and APX-C-labeled synapses. In the same volumes, we randomly selected dendrites (>5 μm in diameter), annotated all potential spines from that dendrite in the volume, and classified it as aspiny or spiny, the latter defined as >0.5 spines/μm. Specifically in layers 2/3, where APX-C labeling was densest (see **Results**), we annotated every terminal as APX-C labeled or unlabeled on spines on those dendrites. We defined a 'potential synapse' in our datasets as any membrane to membrane apposition between a labeled axon with any sign of a synapse, either an axonal terminal (see below) or the presence of postsynaptic densities in targets immediately opposed to labeled terminals. We define axonal terminal as a swelling of the axon, often with clearly identified synaptic vesicles (Figure 2). We searched in the immediate vicinity of these axonal swellings to look for postsynaptic targets, which are identified by postsynaptic densities. In addition, for postsynaptic sites with a clear labeled terminal, we searched each postsynaptic site, particularly spines, for evidence of other synaptic contacts (i.e., we look for additional vesicle filled axonal boutons and other postsynaptic densities on the same spine). For measuring diameters of axonal terminals, spines, and glial appositions, we examined electron microscopic stacks and used the largest diameter for that object in the stack. We often relied on XZ or YZ projections as provided by the Knossos annotation software. Finally, we also cross checked our work

by having each synapse independently annotated by at least two of the authors, and only synapses agreed by each judge (which in our case was >99% agreement) were included for analyses.

Statistical analyses (Mann-Whitney, Chi-Square, and Kruskal-Wallis tests) were performed on the data using custom software in Matlab.

## 3 | Results

We injected a dual viral "cocktail" into the posterior medial thalamic nucleus using stereotactic coordinates (POm; Figure 1A). The first AAV construct expressed *cre* recombinase (pENN.AAV1.hSyn.Cre.WPRE.hGH) and the second AAV construct expressed cytoplasmic targeted, *cre*-dependent APEX2 (Lam et al., 2015; Martell et al., 2017);APX-C, Figure 1B). We found that this "intersectional" viral strategy works: vibratome sections viewed with the light microscope and containing the posterior medial nucleus and secondary somatosensory cortex showed dark staining with Di-Amino Benzene (DAB) (Joesch et al., 2016) in the posterior medial nucleus and putative axonal labeling in S2 cortex (Figure 1B, *bottom*). Serial electron microscopy of the posterior medial nucleus revealed thalamic neurons with APX-C labeling throughout their cytoplasm (Figure 1C, *top*) and synapses from axons of these neurons were clearly visualized along with their postsynaptic targets in S2 cortex (Figure 1C *bottom*).

We analyzed all layers from an individual animal with a single injection site to accurately describe synapses from a single population of labeled POm neurons. In our analyses, we did not assume that all posterior medial cells projecting to the second somatosensory cortex in our injection zone were labeled but rather that our sample is fairly representative of the projection.

We used the ATUM approach (Kasthuri, 2015) to section approximately 3000 50 nm sections from a vibratome slice of secondary somatosensory cortex containing all cortical layers (Figure 1C, 1.7 x 1mm x 0.05mm tissue volume). We

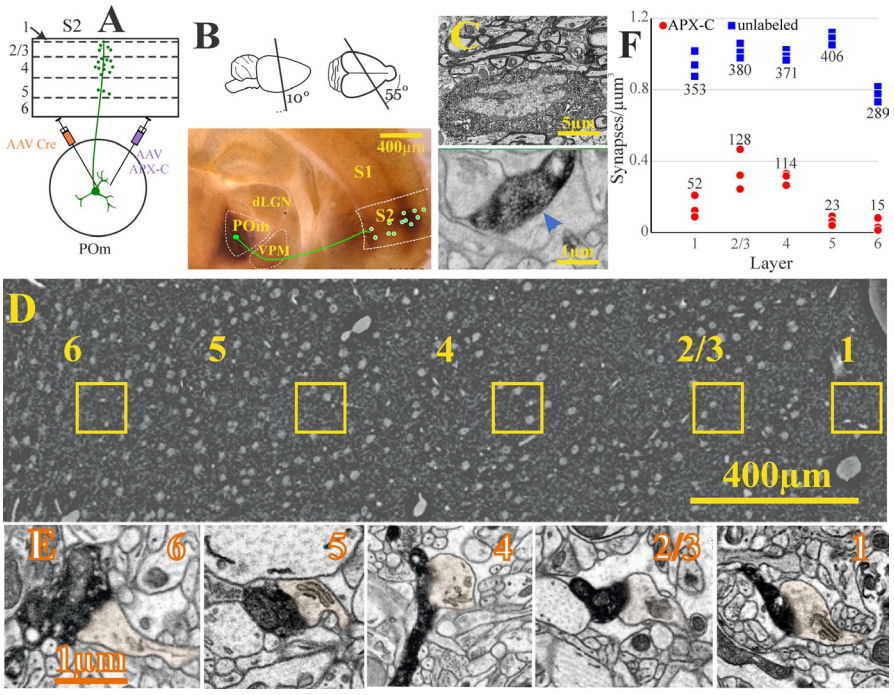


**FIGURE 1** Overview of methodology. (A) We simultaneously injected two types of AAV in the POm of thalamus in wild-type mice: one AAV expressed *cre* recombinase in most or all neurons and a second that expressed APEX2 targeted to the cytoplasm (APX-C) in a cre-dependent fashion. (B) Diagram of slicing angles is shown in top. The bottom shows the APX-C staining. After injections, dark APX-C labeling is clearly visible at the light level in a vibratome slice stained with diaminobenzidine and hydrogen peroxide. The labeling in POm avoids the first-order somatosensory nucleus VPm and the characteristic laminar patterns of POm innervation are visible in S1 and S2 cortex. (C) Electron micrographs showing a POm neuron with the cytoplasm completely filled with APX-C label (*top*) and an APX-C labeled axonal terminal (*bottom*) in S2 (*blue arrow*) (D) We performed multiscale electron microscopy on the resulting sections which spanned the depth of cortex. At lower resolution, we established cortical areas and layers (*numbered)*, and at higher resolution within cortical layers (*yellow boxes*), we reconstructed APX-C labeled and unlabeled synapses. (E) Example synapses onto spines made by APX-C labeled axons from POm in all layers; the layers indicated by the numbers in the upper left corner of each panel. The orange shading denotes postsynaptic spines. (F) Synaptic density (synapses/$\mu m^3$) plots for three volumes separately selected from within each of the yellow boxes in (D). For each volume, every APX-C labeled and unlabeled synapse was identified and counted. The total numbers of synapses for each grouping are also shown

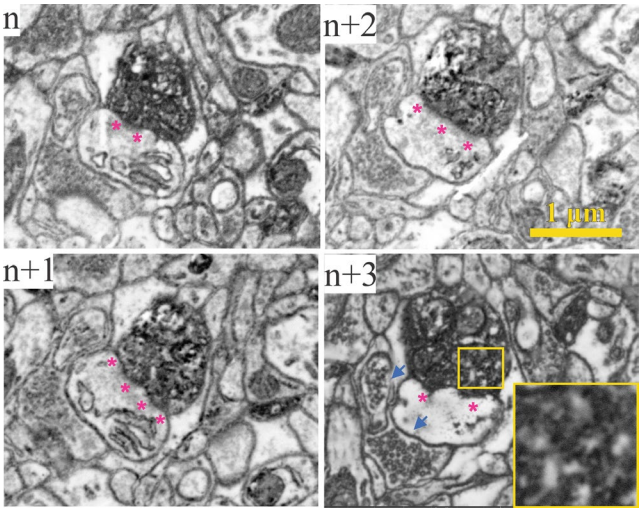


**FIGURE 2** Example of a POm synapse. Shown are four serial electron micrographs (~40 nm thick) of an APX-C labeled synapse onto a spine in layer 4. Purple asterisks mark sites of the postsynaptic density, and synaptic vesicles can be seen in the APX-C labeled terminal (e.g., see slice n+3 and *inset*, which is magnified 2.5 times the rest of the micrographs). Synaptic vesicles in nearby synapses are highlighted by blue arrows for comparison

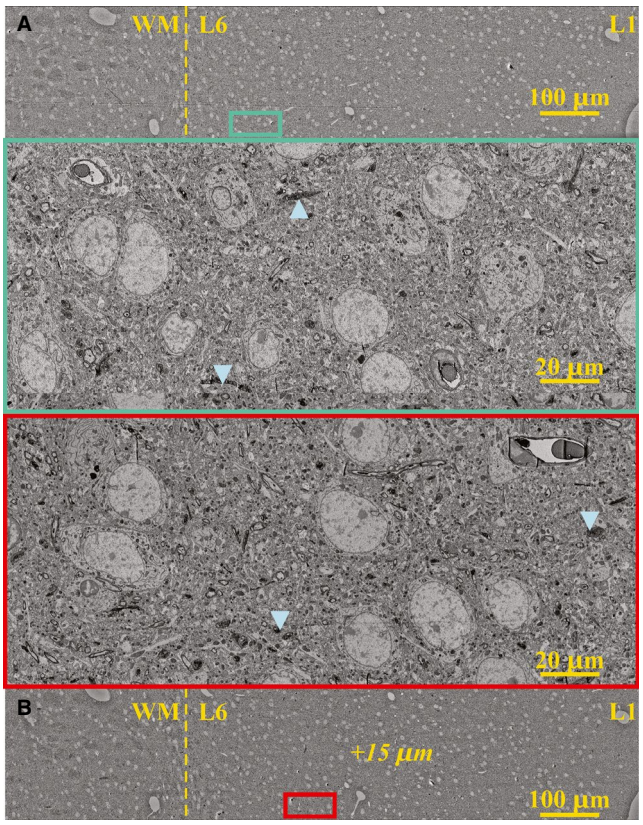


**FIGURE 3** Lack of retrogradely APX-C labeling. Shown are two EM sections ~15 µm apart in a lower-resolution EM stack (40 nm x, y, and z resolution, *top* and *bottom* panels, A and B) of S2 cortex from this dataset. These lower-resolution images show all layers of cortex from layer 1 to white matter (*WM*). Higher-resolution insets within layer 6 are shown from the two labeled fields of view (red and green rectangles). No cell body or dendrite in any layer, and especially layers 5 and 6, showed APX-C labeling throughout the depth of the EM stack (~50 µm thick total). Clear APX-C labeling was seen in myelinated axons (blue arrows) and occasionally in unmyelinated axons (see text)

first performed low-resolution (i.e., 40 nm voxel resolution) serial electron microscopy on ultra-thin sections of cortex in order to identify cortical layers (see **METHODS**) and estimate APX-C labeling density (Figure 1D). We identified zones in each layer (yellow boxes in Figure 1D) for further analysis, and took care to avoid regions near laminar borders. We found axons from the posterior medial nucleus throughout cortex, and closer inspection of the same sections with finer resolution (i.e., 6 nm x & y resolution) showed uniform staining of APX-C even in the finest tips of axons, millimeters away from their cell bodies in thalamus, including clear labeling in layer 1 (Figure 1E). This indicated that the expression of APX-C labels all neuronal processes and overcomes a potential disadvantage of similar experiments with dye injection requiring diffusion of the dye inside the neuron. We then re-imaged five subvolumes of the full cortex dataset at roughly 6 nm x & y resolution for examining the connectivity of labeled thalamocortical axons in each of the cortical layers (Figure 2). As expression depends on a neuron being infected with both viruses, accidental retrograde labeling can be reduced or eliminated. Indeed, we found no labeled cells in cortex, and thus the thalamic injections did not label corticothalamic cells retrogradely (Figure 3).

We found APX-C labeled thalamocortical synapses in all cortical layers. We determined for each layer the relative innervation density of labeled posterior medial synapses relative to all unlabeled synapses. To do this, we reconstructed three small volumes (approximately 125 $\mu m^3$ each; see Methods) in each cortical layer, identified every labeled and unlabeled synapse therein, and calculated synapse density for labeled and unlabeled synapses across cortex (Figure 1F). Even in regions with dense thalamocortical labeling, the synapses from the posterior medial nucleus in every layer were a minority of the synaptic population: based on 2131 total synapses in all layers, 332 APX-C labeled and 1799 unlabeled, we found 0.15 labeled synapse/$\mu m^3$ versus 1 unlabeled synapse/$\mu m^3$ ($p = 2.8E\text{-}12$ on a $\chi^2$-test). We found a laminar relationship for the density of APX-C labeled synapses, with a higher density in layers 2-4 (Figure 1F; $p = 1.3461E\text{-}09$ on a $\chi^2$-test). In contrast, there was no statistically significant laminar relationship for unlabeled synapses ($p = 0.35$ on a $\chi^2$-test). Thus, the relative increased ratio of labeled-to-unlabeled synapses in layers 2-4 was due mainly to the increased density of labeled APX-C synapses in these layers.

We next characterized the frequency at which APX-C labeled terminals in each layer synapsed with dendritic spines

or dendritic shafts and furthermore whether the dendrite was spiny or aspiny (see Methods). We analyzed 1137 APX-C labeled terminals, across all cortical layers (by layer L1: 218, L2/3: 371, L4: 387, L5: 109, L6: 52; Figure 4A,B) and found that only 17 of 1137 synapses from the posterior medial nucleus contacted dendritic shafts. Only 6 of these were on aspiny dendrites; the other 11 were found on dendritic shafts between spines. In order to determine whether this low fraction of innervation on aspiny dendrites (6/1137, 0.53%) reflected an underlying distribution of aspiny dendrites in our dataset, we randomly reconstructed 20 or 21 dendrites in each layer of cortex (Figure 4C). We found that 28% (29/104 dendrites) of the dendrites reconstructed in each layer were aspiny, similar to values reported in the literature (Figure 4D; Sahara et al., 2012). Thus, the low innervation fractions of synapses from the posterior medial nucleus on aspiny dendrites were unlikely to have occurred by chance ($p = 1.1E\text{-}4$ on a $\chi^2$- test) and instead suggests that synapses from the posterior medial nucleus selectively target spiny dendrites.

In order to better appreciate the pattern of thalamocortical connectivity on excitatory neurons, we reconstructed 444 spine synapses onto 21 randomly selected dendritic segments in layers 2/3 of our dataset, thereby sampling the region of highest labeling density (Figure 4B). Of these 21 dendritic segments, 19 received at least one synapse from a posterior medial neuron and 16 received multiple labeled synapses (Figure 4E). As we likely failed to label all neurons of the posterior medial nucleus projecting to the secondary somatosensory cortex, and no other thalamic nuclei were labeled, this is a minimum estimate of the thalamic innervation of this cortical area. We next asked whether the pattern of connectivity onto spines of excitatory dendrites possibly reflected specific targeting by APX-C terminals or could have occurred by chance. APX-C labeled axons innervated 51/444 or 9% of the spines on dendrites in this volume (Figure 4E). We found that the innervation pattern on individual dendrites was consistent with this average. It did not appear that APX-C axons clustered or showed preference for selectively targeting some spiny dendrites and avoiding others. Thus, we could not exclude the possibility that the frequency of APX-C innervation on individual excitatory dendrites differed from chance ($p = 0.35$ on a $\chi^2$-test).

As the majority of APX-C labeled thalamocortical synapses occurred on spines, we next asked whether these spine synapses were distinct from unlabeled synapses on spines throughout all layers. We annotated APX-C and unlabeled

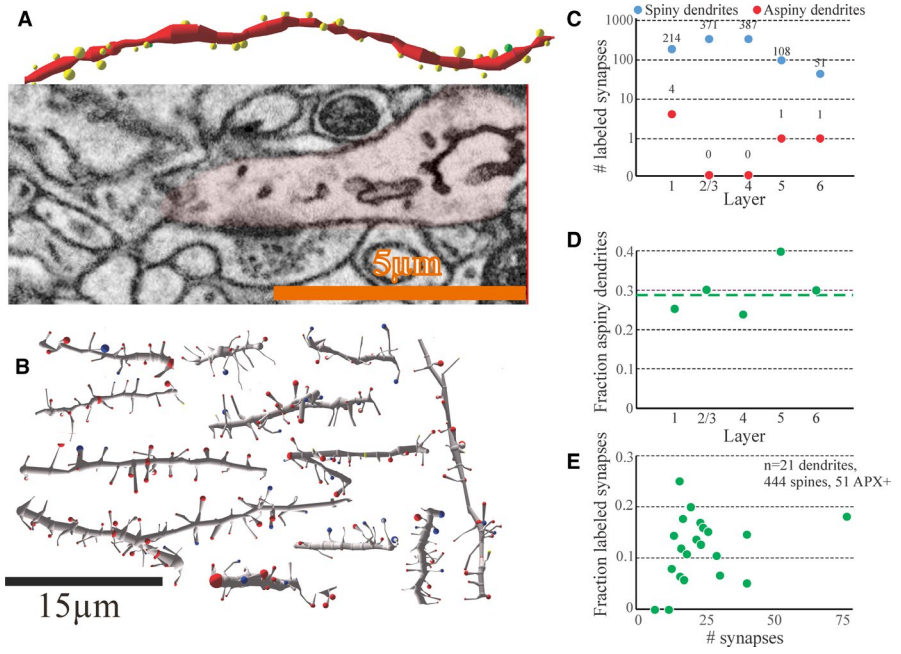


**FIGURE 4** Axons from the posterior medial nucleus selectively target spiny dendrites. We reconstructed APX-C labeled and unlabeled synapses onto dendritic shafts (A) and spines (B) of randomly selected dendrites throughout the layers of S2 cortex. (A) Example reconstruction of an aspiny dendritic segment (red dendrite, *upper*) innervated only by unlabeled synapses where each shaft synapse and its size are annotated (yellow spheres). The single green sphere (*right*) is an unlabeled synapse shown in the electron micrograph below. Synapse density on this dendritic segment was 3 synapses/µm. (B) Example reconstructions of 12 spiny dendritic segments from layers 2/3 where every spine synapse was annotated as APX-C labeled (blue) or unlabeled (red); bouton sizes are also indicated. (C) Plot of the number of synapses made by APX-C labeled boutons on spiny (*blue dots*) and aspiny (*red dots*) dendrites by layer. The number of synapses sampled for each layer is indicated. For every layer, the proportion of APX-C labeled synapses on aspiny dendrites was significantly lower than chance (see text). (D) Plot of fraction of aspiny dendrites randomly selected in each layer. The dashed green line is the average percentage of aspiny dendrites across all layers. (E) The fraction of APX-C labeled synapses on dendritic segments in (B)

synapses randomly throughout each cortical layer (n= 1131 labeled and 891 unlabeled synapses) and focused on six measurements for comparison (Figure 5A): (a) the presence or absence of mitochondria in the terminal (Figure 5B); (b) the presence or absence of "coiled" smooth endoplasmic reticulum in the postsynaptic spine, also known as the spine apparatus ((Spacek, 1985); Figure 5C); (c) the diameter of the postsynaptic spine Figure 5D; (d) the diameter of the pre-synaptic axonal terminal (Figure 5E); (e) the diameter of associated glial processes, if any (Figure 5F); and (f) the number of postsynaptic spines per terminal (Figure 5G). We chose these specific parameters as they have all been implicated in synaptic function (see Discussion).

We found that APX-C labeled synapses are statistically different from unlabeled synapses for each of the above parameters. The labeled synapses derived from larger terminals (1.6 µm mean, 1.5 µm median, for labeled terminals vs. 1.25 µm mean, 1.2 µm median, for unlabeled (Figure 5E; $p$ = 5.05e-15, on a Mann-Whitney $U$-test)) and contacted larger spines (1.26 µm mean, 1.2 µm median, diameter unlabeled spines, 1.6 µm mean, 1.5 µm median, diameter APX-C spines, Figure 5D; $p$ = 2.10E-44, on a Mann-Whitney $U$-test). The posterior medial synapses were more likely to have associated glial processes: of APX-C labeled synapses, 86% (828/964) had an associated glial process, whereas only 53% (296/563) of unlabeled synapses did ($p$ = 8.16E-43 on a $\chi^2$-test). Furthermore, the glial processes at their widest points on labeled synapses were larger, with labeled synapses having a glial diameter of 1.1 µm mean, 1.0 µm median, versus 0.7 µm mean, 0.75 µm median, for unlabeled synapses ($p$ = 1.77E-19, on a Mann-Whitney $U$-test; Figure 5F). Labeled terminals were more likely to synapse with multiple targets (Figure 5G), averaging 1.4 targets versus 1.2 for unlabeled synapses (n=1085 labeled and 863 unlabeled; $p$ = 3.71E-06, on a Mann-Whitney $U$-test). In addition, we randomly annotated 1,545 of all the axonal terminals annotated, 823 labeled and 722 unlabeled, for the presence of mitochondria in the terminal. Of labeled terminals, 78% (644/823) contained a mitochondrion, whereas only 37% (270/722) of unlabeled terminals did so (Figure 5B, $p$ = 7.90E-07 on a $\chi^2$-test). We then randomly analyzed 1994 spines, 1108 innervated by labeled terminals and 886, by unlabeled terminals, for the presence of a spine apparatus. We found that 49% (971/1994) had a prominent spine apparatus. Of spines innervated by labeled terminals, 56% (623/1108) had a spine apparatus, whereas 39% (348/886) of spines associated with unlabeled terminals had a spine apparatus (Figure 5C, $p$ = 4.84E-04 on a $\chi^2$- test).

Finally, we asked how labeled synapses from the posterior medial nucleus differed from unlabeled synapses for the 6 metrics from Figure 5 but now analyzed separately for each cortical layer (Figure 6, see also Table 1). We found that APX-C labeled terminals and synapses differed statistically from unlabeled synapses, with larger values for postsynaptic spine diameter, terminal diameter, associated diameter of glia, presence of mitochondria and postsynaptic spine apparatuses, and number of postsynaptic spines per terminal, in 24 of the 30 comparisons across layers (Mann-Whitney $U$-test and $\chi^2$-test; Table 1). These differences had clear laminar correlations: APX-C labeled synapses showed the largest deviations from unlabeled synapses in layers 2/3, and to a lesser extent in layer 4, and the six comparisons for which we could not statistically distinguish between APX-C and unlabeled synapses occurred in layers 5 and 6. For example, in layers 2/3, APX-C labeled terminals synapsed onto larger spines than did unlabeled terminals: 1.92±.03 µm (mean ± sem; 1.96 µm median) in diameter versus 1.29±.04 µm, 1.33 median, $p$ = 7.09E-27 on a Mann-Whitney $U$-test. Conversely, in layer 6, APX-C labeled terminals contacted spines that were not significantly different in diameter from those contacted by unlabeled terminals (1.47±.06 µm vs. 1.24±.06, 1.35 vs. 1.18 median, $p$ = 0.17 on a Mann-Whitney $U$-test). Moreover, spine diameters contacted by APX-C

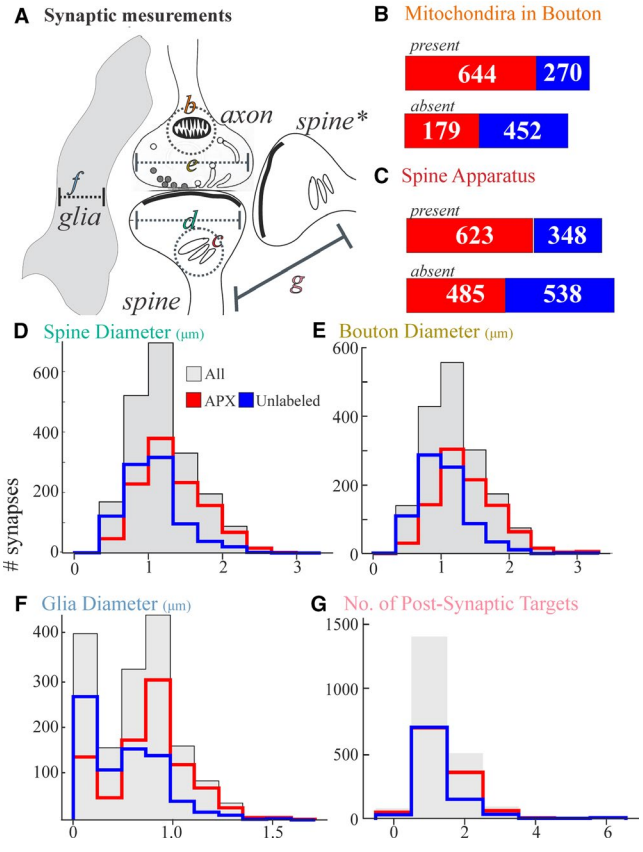


**FIGURE 5** Quantitative differences between APX-C labeled and unlabeled synapses onto spines in cortex. (A) Cartoon parameters measured and illustrated in (B-G). (B) Presence or absence of mitochondria in the presynaptic bouton. (C) The presence of absence of spine apparatus in postsynaptic spines. (D) Maximum spine diameter. (E) Maximum bouton diameter. (F) Maximum diameter of glial process, if present, contacting the synapse. (G) Number of postsynaptic spines innervated by each bouton

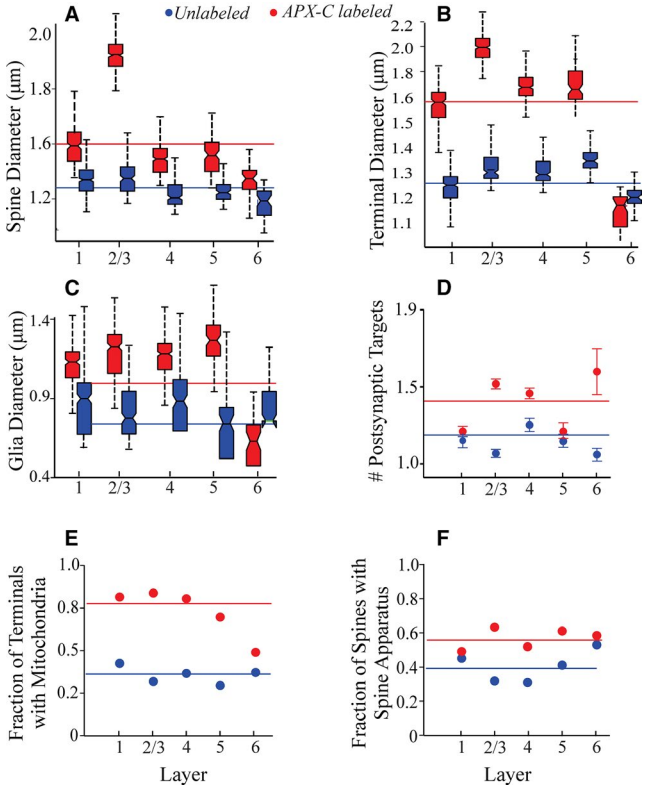


**FIGURE 6** Layer-specific differences between APX-C labeled and unlabeled synapses in cortex. (A-C) Plots showing medians and interquartile ranges. (D) Plot showing means ± SEM. (E-F) Plots showing fraction of synapses. The solid blue and red lines show the mean across all layers for labeled (red lines) and unlabeled (blue lines) synapses

labeled terminals showed clear statistical laminar differences across layers (APX-C spine diameter across layers; $p = 1.2E\text{-}12$, Kruskal-Wallis), whereas those contacted by unlabeled terminals showed no laminar difference in size (p= 0.47 Kruskal-Wallis). We found similar results across the 5 remaining synaptic measures (see Table 1 for statistical values) as follows. The largest differences between APX-C labeled and unlabeled synapses occurred in layers 2/3 (Figure 6A-C). APX-C labeled synapses showed clear laminar differences in the synaptic measures shown in Figure 6A-E, whereas unlabeled synapses showed no such laminar differences. The lone exception to this pattern was the presence of spine apparatuses in postsynaptic profiles (Figure 6F). Although overall, APX-C labeled terminals more frequently contacted spines with spine apparatuses than did unlabeled terminals, this parameter showed a laminar difference for unlabeled terminals but not labeled ones.

## 4 | Discussion

We leveraged advances in automated serial electron microscopy paired with electron-dense genetic labeling using ascorbate peroxidase (APX-C) to analyze long distance connections in a mouse from the posterior medial nucleus of the thalamus to the second somatosensory area of cortex. We found that the labeling strategy works extremely well: clearly labeled synapses in cortex were identified millimeters away from their thalamic cell bodies of origin without signs of reduction in labeling from diffusion or pathological changes to the tissue at the ultrastructural level. We also found that the labeling was orthograde only. This avoids the potential problem of retrograde labeling, which in our case could have labeled corticothalamic cells from layer 5 or 6 and thereby marked local synaptic terminals from these cells, creating false-positive labeling.

However, we recognize at least two provisos in the interpretation of our quantitative analyses. One is that we cannot assume that all thalamocortical cells contributing to the pathway under study were successfully labeled, and of course, other thalamic nuclei innervating the second somatosensory area, such as the ventral posterior nucleus, would have contributed to the population of unlabeled thalamocortical terminals in our study. Related to this, we cannot exclude the possibility that we have labeled a particular population of thalamocortical neurons, and unlabeled ones from the posterior medial nucleus might exhibit properties different from those reported here. It's therefore likely that our analysis undersampled the totality of thalamocortical input. However, the significant differences still found between labeled and unlabeled synapses suggest that the distinctions we highlight here are robust. Additionally, as is common in ultrastructural studies of this type, the analyses are limited to a single animal. We cannot exclude minor individual differences, even among inbred mouse strains.

Figure 7 provides a highly schematized view of much of our work with more details below. Axons of the posterior medial nucleus of the thalamus (POm) innervate all layers of the second somatosensory cortical area (S2). There is laminar variation to this innervation pattern: layers 2/3 receive relatively denser innervation with larger terminals that tend to innervate larger spines, among other measures. In contrast, unlabeled terminals, whose origin is unknown, tend to be smaller and innervate smaller spines, and these terminals show relatively little laminar variation in these parameters.

### 4.1 | Ultrastructural properties of terminals labeled from the posterior medial nucleus

We found labeled synapses from the posterior medial nucleus in every layer of the second somatosensory area. In all layers, labeled terminals specifically targeted spines and spiny dendrites, suggesting a strong preference for innervating excitatory rather than inhibitory cortical neurons (McDonald & Pearson, 1989; Somogyi et al., 1983). While comparing

**TABLE 1** Quantitative details of synaptic input from POm to S2

| **Spine Diameter** | | | | | | | | **Terminal Diameter** | | | | | | |
|---|---|---|---|---|---|---|---|---|---|---|---|---|---|---|
| | Unlabeled | | | APX-C | | | | Unlabeled | | | APX-C | | | |
| Layer | Mean, *n* | Median | SEM | Mean, n | Median | SEM | *p= | Mean, n | Median | SEM | Mean n | Median | SEM | *p= |
| L1 | 1.3, 353 | 1.32 | 0.02 | 1.56, 218 | 1.58 | 0.04 | 1.10E-06 | 1.3, 353 | 1.25 | 0.02 | 1.55, 218 | 1.6 | 0.04 | 2.68E-08 |
| L2/3 | 1.29, 185 | 1.33 | 0.04 | 1.92, 371 | 1.96 | 0.03 | 7.09E-27 | 1.27, 185 | 1.33 | 0.04 | 2.01, 371 | 2 | 0.03 | 1.58E-32 |
| L4 | 1.25, 189 | 1.2 | 0.03 | 1.48, 387 | 1.45 | 0.02 | 3.68E-10 | 1.26, 189 | 1.3 | 0.03 | 1.63, 387 | 1.7 | 0.02 | 8.80E-18 |
| L5 | 1.22, 113 | 1.24 | 0.04 | 1.53, 108 | 1.5 | 0.05 | 3.45E-06 | 1.33, 113 | 1.35 | 0.04 | 1.73, 109 | 1.69 | 0.06 | 5.21E-06 |
| L6 | 1.24, 52 | 1.18 | 1.47 | 1.47, 52 | 1.35 | 0.06 | 0.1696 | 1.17, 52 | 1.2 | | 1.07, 52 | 1.15 | 0.09 | 0.05 |
| | †$p = 0.47$ | | | †$p = 1.2E-12$ | | | | †$p = 0.21$ | | | †$p = 8.8E-6$ | | | |
| **Glia Width** | | | | | | | | **No. of mitochondria** | | | | | | |
| | Unlabeled | | | APX-C | | | | | Unlabeled | | APX-C | | | |
| Layer | Mean, n | Median | SEM | Mean, n | Median | SEM | *p= | | PRESENT | ABSENT | PRESENT | ABSENT | | §p= |
| L1 | 0.84, 353 | 0.9 | 0.03 | 1.1, 218 | 1.2 | 0.04 | 1.20E-04 | | 126 | 170 | 153 | 35 | | 1.72E-04 |
| L2/3 | 0.69, 185 | 0.74 | 0.03 | 1.32, 371 | 1.36 | 0.05 | 1.45E-13 | | 38 | 81 | 154 | 30 | | 1.04E-05 |
| L4 | 0.78, 189 | 0.87 | 0.03 | 1.17, 387 | 1.27 | 0.05 | 0.0025 | | 58 | 100 | 250 | 61 | | 2.54E-18 |
| L5 | 0.74, 113 | 0.8 | 0.03 | 1.23, 109 | 1.3 | 0.05 | 0.0013 | | 29 | 69 | 62 | 27 | | 4.94E-06 |
| L6 | 0.51, 52 | 0.6 | 0.02 | 0.6, 52 | 0.55 | 0.02 | 0.4347 | | 19 | 32 | 25 | 26 | | 0.23 |
| | †$p = 0.16$ | | | †$p = 1.8E-5$ | | | | | §$p = 0.32$ | | §$p = 0.011$ | | | |
| **No. of Postsynaptic Targets** | | | | | | | | **Spine Apparatus** | | | | | | |
| | Unlabeled | | | APX-C | | | | | Unlabeled | | APX-C | | | |
| Layer | Mean, n | Median | SEM | Mean, n | Median | SEM | *p= | | PRESENT | ABSENT | PRESENT | ABSENT | | §p= |
| L1 | 1.15, 353 | 1.1 | 0.05 | 1.23, 218 | 1.28 | 0.03 | 1.93E-10 | | 158 | 193 | 101 | 105 | | 1.87E-07 |
| L2/3 | 1.09, 185 | 1.2 | 0.02 | 1.55, 371 | 1.6 | 0.03 | 8.93E-18 | | 59 | 126 | 232 | 135 | | 7.7E-10 |
| L4 | 1.26, 189 | 1.33 | 0.03 | 1.46, 387 | 1.52 | 0.03 | 3.14E-05 | | 58 | 129 | 198 | 184 | | 2.02E-04 |
| L5 | 1.15, 113 | 1.25 | 0.04 | 1.23, 109 | 1.13 | 0.05 | 0.62 | | 46 | 66 | 64 | 41 | | .0034 |
| L6 | 1.08, 52 | 1.15 | 0.04 | 1.63, 52 | 1.58 | 0.14 | 4.50E-04 | | 27 | 24 | 28 | 20 | | 0.59 |
| | †$p = 0.19$ | | | †$p = 2.1E-4$ | | | | | §$p = \$ 0.023$ | | §$p = 0.14$ | | | |
| Statistical Tests: | | | * Mann-Whitney *U* | | | | §$\chi^2$ | | †Kruskal-Wallis | | | | | |

Statistical tests at the end of rows in the table are comparisons between labeled and unlabeled synapses in that layer for that measure. Statistical tests at the end of columns are comparisons of either labeled or unlabeled synapses across layers for that measure.

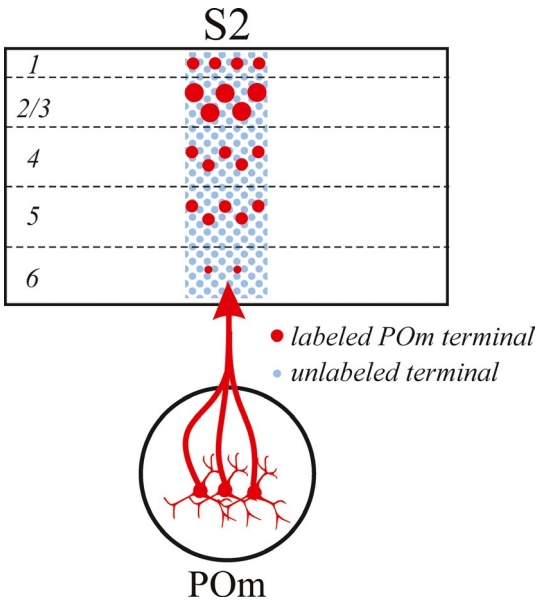


**FIGURE 7** Cartoon summary of results. See text for details

ultrastructural data with physiology and light-level anatomy can be difficult, this result is surprising given that thalamic projections to primary cortical areas affect cortical activity through monosynaptic connections with both excitatory and inhibitory cells (Kloc & Maffei, 2014; Wall et al., 2016). There is, however, some precedent for this result. A previous ultrastructural study showed that thalamocortical projections avoid inhibitory neurons in layer 4 of M1 (Bopp et al., 2017), and a recent comparison of terminals from the posterior medial nucleus to primary motor and primary somatosensory cortices also determined that there were very few labeled terminals on inhibitory interneurons in motor cortex (Rodriguez-Moreno et al., 2020). Combined with the current findings, this observation may represent a difference for higher-order thalamic nuclei projecting to primary or higher-order cortical areas. That is, higher-order thalamocortical projections to motor cortex and higher-order sensory areas, projections that densely innervate layer 4 of cortex and display the properties of glutamatergic driver synapses (Mo & Sherman, 2019), largely avoid monosynaptic connections with inhibitory interneurons; whereas higher-order thalamic projections to primary sensory cortex, projections that densely innervate layers 5 and 1 and display the properties of glutamatergic modulator synapses (Viaene et al., 2011) target both excitatory and inhibitory postsynaptic targets.

Furthermore, the parameters of these labeled synapses varied with layer: layers 2/3 received the largest relative number of terminals from the posterior medial nucleus, and layer 6, the smallest. Labeled synapses in layers 2/3 also had larger terminals and targeted larger spines than did those in other layers (summarized in Figure 7). Finally, other common properties of the labeled thalamocortical terminals included the presence of mitochondria, the presence of spine apparatuses in their postsynaptic spine targets, and the presence of a relatively thick glial wrapping.

The synaptic metrics measured here have known functional implications. The size of postsynaptic spines is associated with spine stability over time and spine size has a strong, positive linear relationship with the magnitude of synaptic currents (Holler-Rickauer et al., 2019). Mitochondria in the bouton serve potentially important roles in vesicle recycling, enhancing short-term plasticity, and stabilizing synaptic connections over time and often suggest highly active terminals (Cserép et al., 2018; Feldman & Peters, 1978; Lees et al., 2020). The presence of a spine apparatus in spine is correlated with potentiated synapses (Deller et al., 2003; Jedlicka et al., 2009). Finally, increasing evidence suggests that glia interact with neurons directly at synapses to modify synaptic function (Eroglu & Barres, 2010). Overall, our anatomical findings strongly suggest that thalamocortical synapses from the posterior medial nucleus to the second somatosensory cortex tend to be functionally more robust and stable than other synapses, which is consistent with limited evidence that these synapses are glutamatergic drivers (Lee & Sherman, 2008; Viaene et al., 2011b).

## 4.2 | Differences between labeled and unlabeled terminals

The labeled terminals differed from unlabeled ones along a number of parameters. For one thing, unlike the labeled synapses, unlabeled ones showed very little evidence of laminar variations in the parameters we measured. Overall, compared to unlabeled terminals, labeled terminals were larger, targeted larger spines that more frequently had spine apparatuses, more often targeted multiple spines, more often had mitochondria, and tended to be associated with larger glial profiles. Because of the variation in layering with these parameters for labeled terminals, the differences between labeled and unlabeled terminals were greatest in layers 2/3.

## 4.3 | On difference between first- and higher-order somatosensory thalamocortical projections

One of our observations for the higher-order somatosensory projection is that labeled terminals are significantly larger in layers 2/3 than in layer 4. This is in stark contrast to the first-order projections from the ventral posterior nucleus to the primary somatosensory cortex and the ventral division of the medial geniculate nucleus to the primary auditory cortex in which the terminals in layer 4 were described as significantly larger than those in layers 2/3 (Viaene et al., 2011a). This is

in keeping with a presumed important functional difference between these first- and higher-order thalamocortical projections. In the first-order projection, thalamocortical inputs to layers 4-6 are all glutamatergic drivers, whereas those to layers 2/3 are mostly glutamatergic modulators, in keeping with the smaller size of thalamocortical terminals in layers 2/3 (Viaene et al., 2011a). This suggests that, whereas most first-order thalamocortical somatosensory and auditory inputs to layers 2/3 are modulators, in the higher-order somatosensory projection, most or all may be drivers.

## 5 | Conclusions

We draw two main conclusions from this work. First, our use of an intersectional viral tracing method for ultrastructural connectivity offers many advantages, including more complete electron-dense labeling compared to labeling often seen with intracellular diffusion of various dyes, and the orthograde labeling we achieved with this technology is free of artifacts often presented by unwanted and uncontrolled retrograde labeling seen with most dye labeling. Our approach is amenable to more general ultrastructural studies of long pathways in the central nervous system.

Second, we believe that this is the first detailed ultrastructural study of this higher-order thalamocortical pathway. Most studies to date have targeted projections to primary sensory cortices, such as from the lateral geniculate nucleus to primary visual cortex (Ahmed et al., 1994; Anderson et al., 2009; Hornung & Garey, 1981; Peters & Feldman, 1977; Peters et al., 1976) and from the ventral posterior nucleus to the primary somatosensory cortex (Bopp et al., 2017; Hersch & White, 1981; Rah et al., 2013; Rodriguez-Moreno et al., 2018; White & Rock, 1979; White et al., 2004). The few published studies of higher-order thalamocortical projections we could find (e.g. Chomsung et al., 2010; Zhou et al., 2018) concentrated on other more specific issues rather than the connectomics analysis of the present study. If we are to gain a better understanding of thalamocortical functioning writ large, we need more descriptions of higher-order thalamocortical examples. Indeed, we have above documented some clear differences between first- and higher-order somatosensory thalamocortical circuits that suggest important functional differences between them.

More generally, it is important to gain a broader understanding of higher-order thalamocortical functioning. First-order thalamic nuclei, such as the lateral geniculate nucleus and ventral posterior nucleus, and their projections to cortex have been relatively well studied. These nuclei relay information from the periphery to cortex (e.g., from the retina for the lateral geniculate nucleus and from the medial lemniscus for the ventral posterior nucleus). In contrast, higher-order thalamic nuclei such as the posterior medial nucleus relay information already in cortex from layer 5 of one area to another area, and thus play a key role in corticocortical communication (reviewed in Sherman, 2016; Sherman & Guillery, 2013)). It is thus especially important to gain a better understanding of these higher-order circuits.

Finally, we are confident in our annotation of synapses, as we independently verified each synapse with at least two scientists. However, if we have miscounted or annotated spines, it is likely that it is the smallest synapses that are potentially missed. These represent a small proportion of the >1000 synapses analyzed, ~10-15 %. The bulk of our results point to differences in POm innervation in the numbers of large synapses (Figure 4) across cortical layers, which we feel are less likely to suffer from potential misinterpretation of small synapses. Thus, even these potential errors in identifying synapses should have little effect on our results. Indeed, as much of our analyses are comparisons of POm synapses across layers, and such errors, if they occur, will occur in all layers. Our robust statistical results in these comparisons strongly suggest that that is not an issue in these analyses.

We view the current study as a bare beginning of an attempt to broaden our understanding of thalamocortical circuitry and the functioning of higher-order thalamocortical pathways. While a great deal more study of this issue is warranted, we hope that the strategy of combining virally mediated labeling with high-throughput electron microscopy contributes to our understanding of previously understudied projections in the brain.

## 6 | COMPETING INTERESTS

The authors have no competing financial interests to divulge.

### ACKNOWLEDGEMENTS

N.K. and V.S. are supported from a technical award from the McKnight foundation, a Brain Initiative of the National Institutes of Health (U01 MH109100), and National Science Foundation Neuro Nex grant. A.M.-H. and S.M.S. are supported by a National Institutes of Health grant from the NINDS (NS094184) and NEI (EY022388). N.K. and S.M.S. are supported by a National Institutes of Health grant from the NINDS (NS113922). Finally, A.M.-H. is supported a National Institutes of Health grant from the NEI (EY028812).

### AUTHOR CONTRIBUTIONS

N.K. and S.M.S. designed research; V.S., A.M.-H., and N.K. performed research; all authors analyzed data and wrote the study.

### PEER REVIEW

The peer review history for this article is available at https://publons.com/publon/10.1111/ejn.15092.

## DATA AVAILABILITY STATEMENT

All authors will be responsible for overseeing the regular backup of the data from their laboratories. We will comply with the NIH Data Sharing requirement (http://grants.nih.gov/grants/policy/data_sharing). All tools (data, assays, libraries, research tools, reagents, etc.) will be made available, in accordance with the policy. Our practices are as follows:

- All datasets made available for sharing in accord with NIH timeliness guidelines. "no later than the date of acceptance for publication of the main findings from the final dataset."
- Data will be shared via electronic transfer or shipping of hard drives, etc., as required on request.
- Datasets shall consist of electronic copies of raw EM images, all annotations, protocols of injections, sequences for viruses, etc.
- All code (MATLAB) will be shared on request.

## ORCID

*Vandana Sampathkumar* https://orcid.org/0000-0002-0577-7164
*S. Murray Sherman* https://orcid.org/0000-0002-1520-2778

## REFERENCES

Agmon, A., & Connors, B. (1991). Thalamocortical responses of mouse somatosensory (barrel) cortex in vitro. *Journal of Neuroscience*, *41*, 365–379.

Ahmed, B., Anderson, J. C., Douglas, R. J., Martin, K. A., & Nelson, J. C. (1994). Polyneuronal innervation of spiny stellate neurons in cat visual cortex. *Journal of Comparative Neurology*, *341*, 39–49.

Anderson, J. C., da Costa, N. M., & Martin, K. A. (2009). The W cell pathway to cat primary visual cortex. *Journal of Comparative Neurology*, *516*, 20–35.

Boergens, K. M., Berning, M., Bocklisch, T., Bräunlein, D., Drawitsch, F., Frohnhofen, J., Herold, T., Otto, P., Rzepka, N., Werkmeister, T., Werner, D., Wiese, G., Wissler, H., & Helmstaedter, M. (2017). webKnossos: efficient online 3D data annotation for connectomics. *Journal of Nature Methods*, *14*, 691–694.

Bopp, R., Holler-Rickauer, S., Martin, K. A., & Schuhknecht, G. F. (2017). An ultrastructural study of the thalamic input to layer 4 of primary motor and primary somatosensory cortex in the mouse. *Journal of Neuroscience*, *37*, 2435–2448.

Cardona, A., Saalfeld, S., Schindelin, J., Arganda-Carreras, I., Preibisch, S., Longair, M., Tomancak, P., Hartenstein, V., & Douglas, R. J. (2012). TrakEM2 software for neural circuit reconstruction. *Journal of PloS One*, *7*.

Chomsung, R. D., Wei, H. Y., DayBrown, J. D., Petry, H. M., & Bickford, M. E. (2010). Synaptic organization of connections between the temporal cortex and pulvinar nucleus of the tree shrew. *Cerebral Cortex*, *20*, 997–1011.

Cserép, C., Pósfai, B., Schwarcz, A. D., & Dénes, Á. J. E. (2018) Mitochondrial ultrastructure is coupled to synaptic performance at axonal release sites. 5. https://doi.org/10.1523/ENEURO.0390-17.2018

Deller, T., Korte, M., Chabanis, S., Drakew, A., Schwegler, H., Stefani, G. G., Zuniga, A., Schwarz, K., Bonhoeffer, T., Zeller, R., Frotscher, M., & Mundel, P. (2003). Synaptopodin-deficient mice lack a spine apparatus and show deficits in synaptic plasticity. *Proceedings of the National Academy of Sciences*, *100*, 10494–10499.

Eroglu, C., & Barres, B. A. (2010). Regulation of synaptic connectivity by glia. *Nature*, *468*, 223–231.

Feldman, M. L., & Peters, A. (1978). The forms of non-pyramidal neurons in the visual cortex of the rat. *Journal of Comparative Neurology*, *179*, 761–793.

Hersch, S., & White, E. (1981). Quantification of synapses formed with apical dendrites of Golgi-impregnated pyramidal cells: variability in thalamocortical inputs, but consistency in the ratios of asymmetrical to symmetrical synapses. *Neuroscience*, *6*, 1043–1051.

Holler-Rickauer, S., Köstinger, G., Martin, K. A., Schuhknecht, G. F., & Stratford, K. J. (2019) Structure and function of a neocortical synapse. *bioRxiv*.

Hornung, J., & Garey, L. (1981). The thalamic projection to cat visual cortex: ultrastructure of neurons identified by Golgi impregnation or retrograde horseradish peroxidase transport. *Journal of Neuroscience*, *6*, 1053–1068.

Hua, Y., Laserstein, P., & Helmstaedter, M. (2015). Large-volume en-bloc staining for electron microscopy-based connectomics. *Nature Communications*, *6*, 7923.

Jedlicka, P., Schwarzacher, S. W., Winkels, R., Kienzler, F., Frotscher, M., Bramham, C. R., Schultz, C., Bas Orth, C., & Deller, T. (2009). Impairment of in vivo theta-burst long-term potentiation and network excitability in the dentate gyrus of synaptopodin-deficient mice lacking the spine apparatus and the cisternal organelle. *Hippocampus*, *19*, 130–140.

Joesch, M., Mankus, D., Yamagata, M., Shahbazi, A., Schalek, R., Suissa-Peleg, A., Meister, M., Lichtman, J. W., Scheirer, W. J., & Sanes, J. R. (2016). Reconstruction of genetically identified neurons imaged by serial-section electron microscopy. *Elife*, *5*, e15015.

Kasthuri, N., Hayworth, K. J., Berger, D. R., Schalek, R. L., Conchello, J. A., Knowles-Barley, S., Lee, D., Vázquez-Reina, A., Kaynig, V., Jones, T. R., Roberts, M., Morgan, J. L., Tapia, J. C., Seung, H. S., Roncal, W. G., Vogelstein, J. T., Burns, R., Sussman, D. L., Priebe, C. E., … Lichtman, J. W. (2015). Saturated Reconstruction of a Volume of Neocortex. *Cell*, *162*, 648–661.

Kloc, M., & Maffei, A. (2014). Target-specific properties of thalamocortical synapses onto layer 4 of mouse primary visual cortex. *Journal of Neuroscience*, *34*, 15455–15465.

Lam, S. S., Martell, J. D., Kamer, K. J., Deerinck, T. J., Ellisman, M. H., Mootha, V. K., & Ting, A. Y. (2015). Directed evolution of APEX2 for electron microscopy and proximity labeling. *Nature Methods*, *12*, 51–54.

Lee, C. C., & Sherman, S. M. (2008). Synaptic properties of thalamic and intracortical inputs to layer 4 of the first-and higher-order cortical areas in the auditory and somatosensory systems. *Journal of Neurophysiology*, *100*, 317–326.

Lees, R. M., Johnson, J. D., & Ashby, M. C. (2020). Presynaptic boutons that contain mitochondria are more stable. *Journal of Frontiers in Synaptic Neuroscience*, *11*, 37.

Martell, J. D., Deerinck, T. J., Lam, S. S., Ellisman, M. H., & Ting, A. Y. (2017). Electron microscopy using the genetically encoded APEX2 tag in cultured mammalian cells. *Nature Protocols*, *12*, 1792–1816.

McDonald, A. J., & Pearson, J. C. (1989). Coexistence of GABA and peptide immunoreactivity in non-pyramidal neurons of the basolateral amygdala. *Neuroscience Letters*, *100*, 53–58.

Mo, C., & Sherman, S. M. (2019). A sensorimotor pathway via higher-order thalamus. *Journal of Neuroscience*, *39*, 692–704.

Morgan, J. L., Berger, D. R., Wetzel, A. W., & Lichtman, J. W. (2016). The fuzzy logic of network connectivity in mouse visual thalamus. *Cell*, *165*, 192–206.

Motta, A., Berning, M., Boergens, K. M., Staffler, B., Beining, M., Loomba, S., Hennig, P., Wissler, H., & Helmstaedter, M. (2019). Dense connectomic reconstruction in layer 4 of the somatosensory cortex. *Science*, *366*.

Peters, A., & Feldman, M. L. (1977). The projection of the lateral geniculate nucleus to area 17 of the rat cerebral cortex, IV terminations upon spiny dendrites. *Journal of Neurocytology*, *6*, 669–689.

Peters, A., Feldman, M., & Saldanha, J. (1976). The projection of the lateral geniculate nucleus to area 17 of the rat cerebral cortex. II. Terminations upon neuronal perikarya and dendritic shafts. *Journal of Neurocytology*, *5*, 85–107.

Rah, J.-C., Bas, E., Colonell, J., Mishchenko, Y., Karsh, B., Fetter, R. D., Myers, E. W., Chklovskii, D. B., Svoboda, K., & Harris, T. D. (2013). Thalamocortical input onto layer 5 pyramidal neurons measured using quantitative large-scale array tomography. *Frontiers in Neural Circuits*, *7*, 177.

Rodriguez-Moreno, J., Porrero, C., Rollenhagen, A., Rubio-Teves, M., Casas-Torremocha, D., Alonso-Nanclares, L., Yakoubi, R., Santuy, A., Merchan-Perez, A., DeFelipe, J., Lubke, J. H., & Clasca, F. (2020). Area-specific synapse structure in branched posterior nucleus axons reveals a new level of complexity in thalamocortical networks. *Journal of Neuroscience*, *40*, 2663–2679.

Rodriguez-Moreno, J., Rollenhagen, A., Arlandis, J., Santuy, A., Merchan-Pérez, A., DeFelipe, J., Lübke, J. H., & Clasca, F. (2018). Quantitative 3D ultrastructure of thalamocortical synapses from the "lemniscal" ventral posteromedial nucleus in mouse barrel cortex. *Cerebral Cortex*, *28*, 3159–3175.

Sahara, S., Yanagawa, Y., O'Leary, D. D., & Stevens, C. F. (2012). The fraction of cortical GABAergic neurons is constant from near the start of cortical neurogenesis to adulthood. *Journal of Neuroscience*, *32*, 4755–4761.

Sherman, S. M. (2016). Thalamus plays a central role in ongoing cortical functioning. *Nature Neuroscience*, *19*, 533.

Sherman, S. M., & Guillery, R. W. (2013). *Functional connections of cortical areas: a new view from the thalamus*, Cambridge, MA: MIT Press.

Somogyi, P., Kisvarday, Z., Martin, K., & Whitteridge, D. (1983). Synaptic connections of morphologically identified and physiologically characterized large basket cells in the striate cortex of cat. *Journal of Neuroscience*, *10*, 261–294.

Spacek, J. (1985). Three-dimensional analysis of dendritic spines. II. Spine apparatus and other cytoplasmic components. *Journal of Anatomy and Embryology*, *171*, 235–243.

Viaene, A. N., Petrof, I., & Sherman, S. M. (2011a). Synaptic properties of thalamic input to layers 2/3 and 4 of primary somatosensory and auditory cortices. *Journal of Neurophysiology*, *105*, 279–292.

Viaene, A. N., Petrof, I., & Sherman, S. M. (2011b). Properties of the thalamic projection from the posterior medial nucleus to primary and secondary somatosensory cortices in the mouse. *Proceedings of the National Academy of Sciences*, *108*, 18156–18161.

Wall, N. R., De La Parra, M., Sorokin, J. M., Taniguchi, H., Huang, Z. J., & Callaway, E. M. (2016). Brain-wide maps of synaptic input to cortical interneurons. *Journal of Neuroscience*, *36*, 4000–4009.

White, E., & Rock, M. (1979). Distribution of thalamic input to different dendrites of a spiny stellate cell in mouse sensorimotor cortex. *Neuroscience Letters*, *15*, 115–119.

White, E. L., Weinfeld, E., & Lev, D. L. (2004). Quantitative analysis of synaptic distribution along thalamocortical axons in adult mouse barrels. *Journal of Comparative Neurology*, *479*, 56–69.

Zhou, N., Masterson, S. P., Damron, J. K., Guido, W., & Bickford, M. E. (2018). The mouse pulvinar nucleus links the lateral extrastriate cortex, striatum, and amygdala. *Journal of Neuroscience*, *38*(2), 347–362.

**How to cite this article:** Sampathkumar V, Miller-Hansen A, Murray Sherman S, Kasthuri N. An ultrastructural connectomic analysis of a higher-order thalamocortical circuit in the mouse. *Eur J Neurosci*. 2021;53:750–762. https://doi.org/10.1111/ejn.15092